Mat. Res. Bull., Vol. 19, pp. 817-824, 1984. Pergamon Press Ltd.
0025-5408/84 $3.00 + .00

PHOTOELECTROCHEMICAL PROPERTIES OF $MgTiO_3$ AND OTHER TITANATES WITH THE ILMENITE STRUCTURE

L.G.J. de Haart, A.J. de Vries and G. Blasse
Physical Laboratory, State University,
P.O. Box 80.000, 3508 TA Utrecht, The Netherlands

(Received March 12, 1984; Communicated by P. Hagenmuller)

ABSTRACT

The photoelectrochemical properties and the diffuse reflection spectrum of $MgTiO_3$ are reported. $MgTiO_3$ shows an optical absorption edge near 3.7 eV. This makes the material unsuitable for solar energy applications. The diffuse reflection spectra of $CoTiO_3$ and $MnTiO_3$ are presented. The optical absorption edge shifts to lower energy due to the occurrence of $Me^{2+} \rightarrow Ti^{4+}$ charge-transfer transitions. For various reasons discussed no photocurrents were observed for $CoTiO_3$ and $MnTiO_3$.

Introduction

Extensive studies have been carried out to find the most suitable photoelectrode material for the photoelectrolysis of water. Many n-type semiconductor anodes for the one-step photoelectrolysis of water have been investigated (1), but unfortunately either the material corrodes under illumination, or it does not respond to visible light irradiation. For the stable wide-bandgap materials TiO_2 and $SrTiO_3$ ($E_g \geqslant 3$ eV) doping with various transition-metal ions has been shown to increase the photoresponse into the visible part of the solar spectrum (2,3). However, these transition-metal ions form localized levels in the forbidden bandgap, leading to low mobility for the associated holes. Consequently a large bias is required to get a significant photoresponse in the visible (3). The introduced transition-metal ions cannot form an electronic subband, because together with the Ti^{4+} ions they occupy the same sublattice. Therefore Goodenough et al. (4) suggested to use a mixed metal oxide in which each band is associated with a different cation. The crystal structure of this oxide must contain two different metal ions each occupying one sublattice. The compounds $MeTiO_3$ ($Me^{2+} = Mg^{2+}$, Mn^{2+}, Fe^{2+}, Co^{2+}, Ni^{2+}) which have the ilmenite structure fulfill this requirement. The ilmenite structure (5) can be considered as an ordered corundum structure with Me^{2+} and Ti^{4+} ions in alternating layers perpendicular to the c axis of

the unit cell. Both cations are octahedrally coordinated by oxygen and within each layer these octahedra share edges, so that band formation is possible.

De Korte and Blasse (6) and Salvador, Gutierrez and Goodenough (7-9) have shown that $NiTiO_3$ acts indeed as a semiconducting anode in water photoelectrolysis. Between the 2p valence band of oxygen and the 3d conduction band of titanium a narrow cationic (Ni^{2+}:$3d^8$) band is situated. There is, however, a difference in the spectral interpretation between the work of De Korte and Blasse and the work of Salvador et al., as the former authors already pointed out (6). De Korte and Blasse based their work on data for $MgTiO_3$ which were not used by Salvador et al.

Recently Bin-Daar et al. (10) reported the properties of $MnTiO_3$ as a photoanode capable of water splitting. These authors also did not base their work on data for $MgTiO_3$.

In view of this we report here the optical and photoelectrochemical properties of $MgTiO_3$ and we review the optical properties of several titanates $MeTiO_3$ (Me^{2+} = Mn^{2+}, Fe^{2+}, Co^{2+}, Ni^{2+}) with the ilmenite structure.

Experimental

Samples were prepared by usual ceramic techniques using high-purity starting materials. The TiO_2 used in these preparations was obtained by thermal decomposition of ammoniumtitaniumoxalate $[(NH_4)_2TiO(C_2O_4)_2.H_2O]$ at 1000 °C. Firing of the samples was performed between 1100 °C and 1200 °C in air (Me = Mg, Co) or in a nitrogen/hydrogen (N_2:H_2 = 3:1) atmosphere (Me = Mn). Samples were checked by X-ray powder diffraction. Diffuse reflection spectra were recorded at room temperature on a Perkin-Elmer EPS-3T spectrophotometer.

The powders were cold-pressed at 100-150 kg/cm^2 and subsequently sintered at 1200 °C to 1300 °C. The pellets were polished and again fired in a reducing atmosphere. This reducing atmosphere could be a CO/CO_2 mixture, N_2/H_2 mixtures or pure hydrogen. The $MgTiO_3$ and the $MnTiO_3$ samples were doped with 1 % of niobium. The surfaces of the pellets were examined for their structure and composition with a Cambridge Stereo Scan 150 electron microscope, equipped with an energy dispersive elementary analysis apparatus (Link Systems, U.K.).

The cell arrangement and electrochemical measurement procedures have been described previously (3). Electrode potentials are referred to a saturated calomel electrode (SCE). All photoelectrochemical measurements were carried out in 1 N NaOH.

Results

In Figure 1 the diffuse reflection spectra of $MgTiO_3$, $CoTiO_3$, $MnTiO_3$ and of $MgTiO_3$ doped with 0.5 mol % Cr^{3+} are presented. The optical absorption edge of $MgTiO_3$ is situated at about 335 nm (3.7 eV). In addition there is a tail in the spectrum which extends into the visible region. The $CoTiO_3$, $MnTiO_3$ and Cr-doped $MgTiO_3$ samples are heavily coloured; their reflection spectra are dominated by broad intense absorptions in the visible region. We were not able to prepare single phase $FeTiO_3$ by usual ceramic techniques.

The net photocurrent density as a function of the wavelength of the irradiated light is shown in Figure 2 for a $MgTiO_3$ and a $MgTiO_3$ - 0.5 % Cr^{3+} electrode. The measurements were carried out with zero bias voltage (vs SCE).

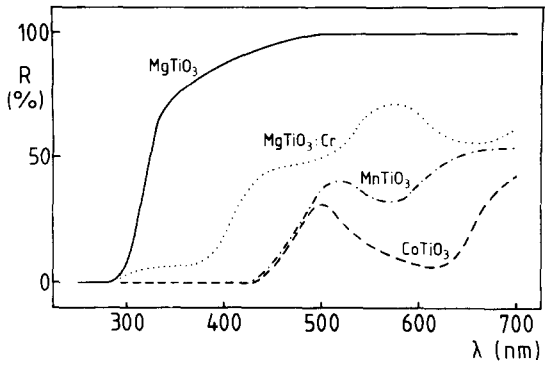

FIG. 1

Diffuse reflection spectra of $MgTiO_3$, $CoTiO_3$, $MnTiO_3$ and of $MgTiO_3$-0.5 % Cr at room temperature. MgO was used as a standard reference.

We remark that our equipment for measuring photocurrents is limited on the short-wavelength side to 300 nm. The $MgTiO_3$ electrode showed very low photocurrents, the onset wavelength being around 370 nm. The photocurrents observed for the Cr-doped $MgTiO_3$ electrode were even lower, the onset wavelength, however, shifted to a longer value, viz. 420 nm.

Figure 3 shows the net photocurrent density as a function of the applied potential (vs SCE) for a $MgTiO_3$ electrode. The incident monochromatic light had a wavelength of 300 nm. For other wavelengths a similar behaviour was observed. The onset potential is at about -0.7 V vs SCE. The photocurrent rises slowly with increasing potential and tends to reach saturation at potentials above 1.0 V vs SCE.

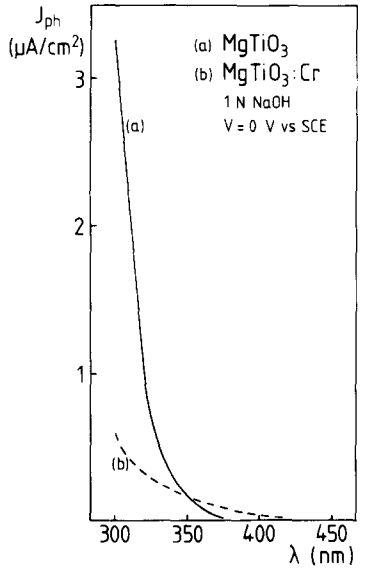

FIG. 2

Variation of photocurrent density with irradiation wavelength for $MgTiO_3$ and for $MgTiO_3$-0.5 % Cr.

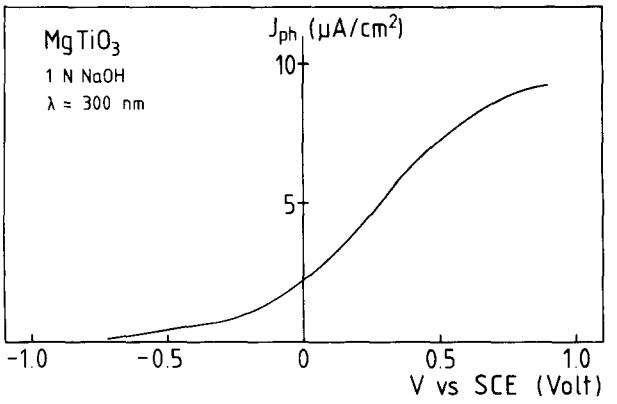

FIG. 3

Variation of photocurrent density with applied potential (vs SCE) for $MgTiO_3$.

The $MgTiO_3$ and Cr-doped $MgTiO_3$ electrodes had a density ratio of 90 % after sintering. By doping with 1 % of niobium and subsequently firing in a hydrogen atmosphere a resistivity of 5 k Ω was obtained. In Figure 4, a representative scanning electronmicrograph is shown of the surface of a $MgTiO_3$ electrode. X-ray diffraction showed no decomposition of the surface.

The density ratio of the $CoTiO_3$ pellets was 83 % after sintering. Firing in a slightly reducing CO/CO_2 atmosphere did not lower the resistivity sufficiently. X-ray diffraction showed partial decomposition of the surface. Firing in a more reducing H_2/N_2 atmosphere lowered the resistivity to around 10 Ω. Figure 5 shows a scanning electronmicrograph of the surface of a $CoTiO_3$ pellet after this reduction treatment. A large number of pits is present on the surface after reduction. Scanning electronmicrographs of these pits taken with further enlargement are shown in Figure 6. In this figure are inserted the results of scans on Co and Ti over the horizontal line shown in the graphs. For none of the $CoTiO_3$ electrodes photocurrents were observed.

For the $MnTiO_3$ pellets a density ratio of 90 % was obtained after sintering. After reduction in pure hydrogen at 1000 °C the resistivity remained very high (> 1 M Ω), even when the material was doped with 1 % of niobium. X-ray diffraction showed no decomposition of the surface. No photocurrents were observed for these $MnTiO_3$ electrodes.

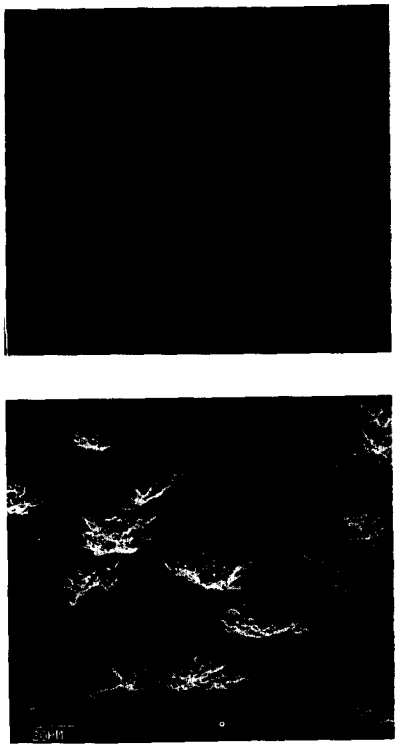

FIG. 5

Scanning electronmicrograph of the surface of a $CoTiO_3$ disk after reduction in a H_2/N_2 atmosphere.

FIG. 4

Scanning electromicrograph of the surface of a $MgTiO_3$ electrode.

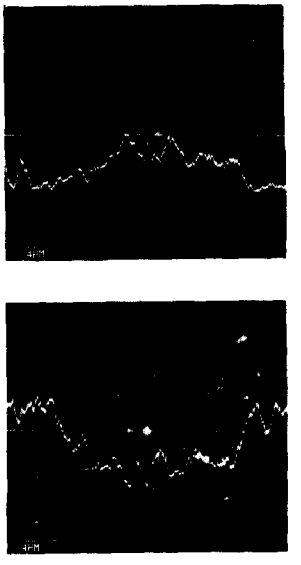

FIG. 6

Scanning electronmicrographs of the surface of a $CoTiO_3$ disk with scans on Co (above) and on Ti (below).

Discussion

The bandgap of $MgTiO_3$ (3.7 eV) is much larger than that of $SrTiO_3$ (3.2 eV) or TiO_2 (3.0 eV). This makes the material clearly unsuitable for solar energy conversion. The absorption is due to an $O^{2-} \rightarrow Ti^{4+}$ charge-transfer (C.T.) transition. The tail in the reflection spectrum of $MgTiO_3$ will be discussed below.

In $CoTiO_3$ and $MnTiO_3$ the optical absorption edge is shifted to lower energy due to the occurrence of the $Me^{2+} \rightarrow Ti^{4+}$ C.T. transitions. For both materials the band edge is situated at 510 nm (2.4 eV) (see Figure 1). For $NiTiO_3$ a shift of the band edge to 450 nm (2.8 eV) was observed (6). The onset of the C.T. band is thus at lower energy for Co^{2+} and Mn^{2+} than for Ni^{2+}. According to the model of Blasse et al. (11), this is in good agreement with the 3rd ionization potentials of these ions [Ni: 35.2 eV, Co: 33.5 eV, Mn: 33.7 eV (12)]. For Co^{2+} the spin-allowed crystal-field transition is clearly visible at about 610 nm. Assignment of the band at 570 nm in the spectrum of $MnTiO_3$ is less obvious. It is not expected that the spin- and parity-forbidden crystal-field transitions on Mn^{2+} can be observable in this type of spectra. It is possible that a certain amount of Mn^{3+} is present, so that this band may be the $^5E \rightarrow {}^5T_2$ transition on Mn^{3+} (ref. 13). Apart from this absorption band, the spectra of $CoTiO_3$ and $MnTiO_3$ are in good agreement with the reflection spectra of Co^{2+} and Mn^{2+} doped $MgTi_2O_5$ reported by Blasse and Dirksen (14), bearing in mind, that the latter are spectra of diluted systems.

The diffuse reflection spectrum of Cr^{3+}-doped $MgTiO_3$ shows the expected $Cr^{3+} \rightarrow Ti^{4+}$ C.T. transition up to around 480 nm (see Figure 1). Around 480 nm and 660 nm the crystal-field transitions on Cr^{3+} are clearly visible: $^4A_2 \rightarrow {}^4T_1$ and $^4A_2 \rightarrow {}^4T_2$, respectively.

It is more or less common to titanates that defect titanate centres, which show absorption on the long-wavelength side of the intrinsic absorption edge, are present (15). Note that a slight disorder between Mg^{2+} and Ti^{4+} in $MgTiO_3$ results in titanate centres, which will be responsible for the tail in the reflection spectrum of $MgTiO_3$. The same phenomenon was observed for the titanate $K_{1.8}Mg_{0.9}Ti_{7.1}O_{16}$ with the hollandite structure (16). Luminescence measurements on the same $MgTiO_3$ samples showed emission from these defect titanate centres (17). For $K_{1.8}Mg_{0.9}Ti_{7.1}O_{16}$ photocurrents were observed for excitation in the intrinsic titanate centres as well as for excitation in the defect titanate centres. In the hollandite structure both titanate centres are on the same sublattice (16). In the case of $MgTiO_3$, however, the defect titanate centre is within the Mg sublattice in the ilmenite structure. Perhaps this titanate centre acts as a recombination centre. No photocurrent will then be observed with excitation in the defect titanate centres. The photocurrent for a $MgTiO_3$ electrode shown in Figure 2 is therefore exclusively due to excitation in the intrinsic titanate absorption band. The photocurrents still observed around 370 nm can be due to the necessary use of the large slits of the monochromator.

The shift of the absorption edge observed when Cr^{3+} is introduced in $MgTiO_3$ amounts to about 9000 cm^{-1}. This is of the same magnitude as in $K_{1.8}Cr_{0.3}Al_{1.5}Ti_{6.2}O_{16}$ (ref. 16). Because of this large energy difference between the Cr^{3+} levels and the top of the oxygen valence band, the Cr^{3+} ions will act as efficient hole traps. Only a very low photocurrent is observed for irradiation with light corresponding with the $Cr^{3+} \rightarrow Ti^{4+}$ C.T. absorption band (see Figure 2). This is well in line with the photocurrent-action spectrum observed for $K_{1.8}Cr_{0.3}Al_{1.5}Ti_{6.2}O_{16}$ (ref. 16).

The slow rise of the photocurrent with increasing potential for a $MgTiO_3$ electrode (see Figure 3) indicates, that at low potentials recombination processes are predominant (18). Recombination will probably take place at the defect titanate centres present in the material. The observed onset potential of the photocurrent (-0.7 V vs SCE) is the same as observed for $NiTiO_3$ by De Korte and Blasse (6). This has to be expected, since both compounds have the ilmenite structure.

In passing we note the following. For TiO_2 (E_g = 3.0 eV) the onset potential is -0.9 V vs SCE (19), for $K_{1.8}Mg_{0.9}Ti_{7.1}O_{16}$ (E_g = 3.4 eV) the onset potential is -0.9 V vs SCE (16) and for $MgTiO_3$ (E_g = 3.7 eV) we found -0.7 V vs SCE, all values corrected to the same pH. The value of the onset potential is a measure for the position of the bottom of the conduction band on the energy scale, neglecting small differences between the bottom of the conduction band and the Fermi level. We conclude that this position is nearly the same for the materials under discussion. The great differences in the bandgaps, i.e. the distance between the bottom of the titanium conduction band and the top of the oxygen valence band, must therefore be fully accounted for by the position of the top of the valence band. The differences may be due to a decrease of the width of the oxygen valence band in the sequence TiO_2, $K_{1.8}Mg_{0.9}Ti_{7.1}O_{16}$, $MgTiO_3$. This will be discussed later in connection with the results of a study on the luminescence of the titanates (17).

The very low resistivity of the $CoTiO_3$ pellets observed after reduction in a H_2/N_2 atmosphere is supposed to be due to the presence of metallic cobalt. During the reduction treatment large pits are formed on the surface as shown in Figure 5. Reduction is thought to take place at these spots and the line-scans on Co and Ti shown in Figure 6 indicate a clustering of Co (metal) inside these pits. Because of this decomposition of the material no photocurrent had to be expected, in agreement with observation.

It is possible that the presence of Mn^{3+} in our $MnTiO_3$ sample impedes the lowering of the resistivity. The authors of ref. (10), however, succeeded in obtaining a conducting $MnTiO_3$ electrode. The diffuse reflection spectrum of their sample showed only feeble absorption above 480 nm. This absorption edge corresponds with the $Mn^{2+} \rightarrow Ti^{4+}$ C.T. transition observed by us and the absence of any absorption above 480 nm indicates that no Mn^{3+} is present. Bin-Daar et al. place the bulk Mn^{2+} level 1.5 eV below the titanium conduction band, based on results obtained for TiO_2 by Mizushima et al. (20). But the reflection spectra show, that this difference is at least 2.2 eV. It was found before, that the position of transition-metal ion levels depends on the bandgap of the host lattice. The position of these levels relative to the conduction band is more affected by an increase of the bandgap than its position relative to the valence band (11, 14, 21).

Only a very small photocurrent was observed by Bin-Daar et al. for $MnTiO_3$ with wavelengths longer than 400 nm. This means that for $Mn^{2+} \rightarrow Ti^{4+}$ C.T. excitation no photocurrents of any importance result. This may be due to the fact that the small polarons in this case correspond to Mn^{3+} ions which might be very immobile due to a Jahn-Teller deformation. The photocurrents observed for white light and UV excitation reported in ref. (10) have a low quantum efficiency (about 1 %). The photocurrent density is of the same order of magnitude as the photocurrent density observed for $MgTiO_3$. Further the potential dependence of the photocurrent for $MnTiO_3$ with white light irradiation resembles the current/voltage characteristic of $MgTiO_3$. Therefore it cannot be excluded that the photocurrents reported by Bin-Daar et al. for $MnTiO_3$ are due to excitation in the edge of the intrinsic titanate absorption band. Their somewhat longer wavelength dependence may be due to the use of different techniques.

Conclusions

For titanates with the ilmenite structure the intrinsic titanate absorption band is situated at 3.7 eV. In the corresponding transition-metal titanates the band edge shifts to lower energy. For $NiTiO_3$ photocurrents were observed with excitation in the $Ni^{2+} \rightarrow Ti^{4+}$ C.T. band. But the band edge (2.8 eV) is still too large for efficient use in a solar cell. For $CoTiO_3$ and $MnTiO_3$ the band edge is situated at 2.4 eV. But $CoTiO_3$ decomposes during reduction and for $MnTiO_3$, excitation in the $Mn^{2+} \rightarrow Ti^{4+}$ C.T. band does not result in photocurrents. The only other candidate left is $FeTiO_3$. Ginley and Butler (22) reported for this compound E_g = 2.6 eV and V_{fb} = -0.6 V vs SCE. These valaues appeared to depend on the degree of ordening of the metal ions in the ilmenite structure. According to these authors $FeTiO_3$ is inferior to Fe_2O_3.

Acknowledgements

The authors are indebted to J. Pieters for performing the electron microscope analaysis.

The investigations were supported by the Netherlands Foundation for Chemical Research (SON) with financial aid from the Netherlands Foundation for Technical Research (STW).

References

1. H.P. Maruska and A.K. Ghosh, Solar Energy 20, 443 (1978)
M.A. Butler and D.S. Ginley, J. Mater. Sci. 15, 1 (1980)
K. Rajeshwar, P. Singh and M. DuBow, Electrochim. Acta 23, 1117 (1978)

2. H.P. Maruska and A.K. Ghosh, Solar Energy Mat. 1, 237 (1979)
Y. Matsumoto, J. Kurimoto, T. Shimizu and E. Sato, J. Electrochem. Soc. 128, 1040 (1981)

3. R.U.E. 't Lam, L.G.J. de Haart, A.W. Wiersma, G. Blasse, A.H.A. Tinnemans and A. Mackor, Mat. Res. Bull. 16, 1593 (1981)

4. J.B. Goodenough, A. Hamnett, M.P. Dare-Edwards, G. Campet and R.D. Wright, Surf. Sci. 101, 531 (1980)

5. R.W.G. Wyckoff, Crystal Structures, 2nd ed., vol. 2, Interscience Publ. New York, 1963

6. P.H.M. de Korte and G. Blasse, J. Solid State Chem. 44, 150 (1982)

7. P. Salvador, C. Gutierrez and J.B. Goodenough, Appl. Phys. Lett. 40, 188 (1982)

8. C. Gutierrez, P. Salvador and J.B. Goodenough, J. Electroanal. Chem. 134, 325 (1982)

9. P. Salvador, C. Gutierrez and J.B. Goodenough, J. Appl. Phys. 53, 7003 (1982)

10. G. Bin-Daar, M.P. Dare-Edwards, J.B. Goodenough and A. Hamnett, J. Chem. Soc., Faraday Trans. 1, 79, 1199 (1983)

11. G. Blasse, P.H.M. de Korte and A. Mackor, J. Inorg. Nucl. Chem. 43, 1499 (1981)

12. Handbook of Chemistry and Physics (R.C. Weast, ed.), 57th edition, CRC Press, Cleveland, 1976

13. A.B.P. Lever, Inorganic Electronic Spectroscopy, Elsevier Publishing Company, Amsterdam, 1968

14. G. Blasse and G.J. Dirksen, Chem. Phys. Lett. 77, 9 (1981)

15. A.J.H. Macke, J. Solid State Chem. 18, 337 (1976)

16. L.G.J. de Haart, G.R. Meima and G. Blasse, Mat. Res. Bull. 18, 203 (1983)

17. A.J. de Vries, L.G.J. de Haart and G. Blasse, to be published

18. R.U.E. 't Lam and D.R. Franceschetti, Mat. Res. Bull. 17, 1081 (1982)

19. M.A. Butler and D.S. Ginley, J. Electrochem. Soc. 125, 228 (1978)

20. K. Mizushima, M. Tanaka, A. Asai, S. Iida and J.B. Goodenough, J. Phys. Chem. Solids 40, 1129 (1979)

21. R.U.E. 't Lam and G. Blasse, Ber. Bunsenges. Phys. Chem. 86, 1150 (1982)

22. D.S. Ginley and M.A. Butler, J. Appl. Phys. 48, 2019 (1977)